AGU PUBLICATIONS

JGR

Journal of Geophysical Research: Oceans

RESEARCH ARTICLE

10.1002/2015JC011056

Key Points:
- Low mineral particle concentrations have important optical effects in shelf seas
- Mineral particles in the Irish Sea exhibit complex spatial and seasonal patterns
- Specific optical properties of mineral particles can be obtained by remote sensing

Correspondence to:
A. Cunningham,
a.cunningham@strath.ac.uk

Citation:
Mitchell, C., A. Cunningham, and D. McKee (2016), Derivation of the specific optical properties of suspended mineral particles and their contribution to the attenuation of solar irradiance in offshore waters by ocean color remote sensing, *J. Geophys. Res. Oceans*, *121*, 104–117, doi:10.1002/2015JC011056.

Received 16 JUN 2015
Accepted 7 DEC 2015
Accepted article online 14 DEC 2015
Published online 8 JAN 2016

Derivation of the specific optical properties of suspended mineral particles and their contribution to the attenuation of solar irradiance in offshore waters by ocean color remote sensing

Catherine Mitchell[1], Alex Cunningham[1], and David McKee[1]

[1]Department of Physics, University of Strathclyde, Glasgow, UK

Abstract Two independently derived algorithms which had previously been validated against in situ data were applied to 8 years of MODIS observations of the Irish Sea to obtain (i) concentrations of lithogenic mineral particles (*MSSl*) in surface waters and (ii) the specific backscattering and absorption coefficients for these particles in the 488 nm waveband (the values obtained were $a^*_{MSSl}488 = 0.031$ m^2 g^{-1} and $b_b{}^*_{MSSl}488 = 0.010$ m^2 g^{-1}). This information was used to calculate the mean attenuation coefficient for downward irradiance $\bar{K}_d(488)$ in the surface mixed layer, and the fraction of this coefficient that was attributable to suspended mineral particles. Mineral particles at relatively low concentrations (<5 g m^{-3}) were the major determinant of $\bar{K}_d(488)$ values throughout the region in winter, and in the central Irish Sea this influence persisted for much of the spring/autumn primary production period. In the north and south, however, marked short-term increases in $\bar{K}_d(488)$ due to phytoplankton blooms occurred during periods when *MSSl* values were relatively low. Seasonally averaged maps of the fractional contribution of MSS*l* to $\bar{K}_d(488)$ show strong links to vertical mixing, with sharp contrasts developing in spring at the boundaries between mixed and stratified waters. We conclude that the ocean color processing sequence presented here can reveal spatial and seasonal patterns in the dynamics of lithogenic mineral particles which have potentially valuable applications in ecosystem status assessment, environmental impact monitoring, and the tuning and validation of numerical models of shelf sea ecosystems.

1. Introduction

Mineral particles in the marine environment can be classified according to their origin as biogenic (mainly calcite and silica structures synthesized by phytoplankton cells) or lithogenic (clays and silicates derived from sedimentary material) [*Zhang et al*., 2014]. Since both classes of particles make significant contributions to the mineral suspended solids (*MSS*) load in UK shelf seas [*Neil et al*., 2011; *Van Oostende et al*., 2012], we use *MSSl* in this paper to designate lithogenic mineral particles. It is widely recognized that these particles are an important determinant of the optical properties of turbid estuaries and shallow coastal waters [*Astoreca et al*., 2012], and optical measurements are routinely employed to study their suspension and transport [*Agrawal and Pottsmith*, 2000; *Downing*, 2006]. Offshore, however, in deeper waters beyond the direct influence of terrestrial inputs, lithogenic minerals are present in lower mass concentrations and much less attention has been paid to assessing their optical and ecological significance [*Kostadinov et al*., 2012].

At first sight, it would appear that this issue could be addressed by a modest program of radiative transfer modeling [*Mobley*, 1994], but such modeling requires accurate knowledge of the concentrations and specific optical properties (*SIOPs*) of mineral particles in the offshore environment. In practice, a surprising degree of difficulty is encountered in obtaining this information. Problems in determining *SIOPs* arise from the need to use statistical regression or cluster analysis to distinguish between scattering from lithogenic minerals and other particles in natural mixtures [*Babin et al*., 2003; *McKee and Cunningham*, 2006; *Stavn and Richter*, 2008], and to a lesser extent from the possible alteration of the physical state of the particles during collection and filtration [*Lunau et al*., 2004]. Difficulties in ascertaining particle concentrations are partly due to the high degree of spatial variability found in shelf seas, and partly to the fact that research cruises rarely sample these waters in winter when sediment resuspension is most active [*Bowers*, 2003; *Fettweis and Nechad*, 2011].

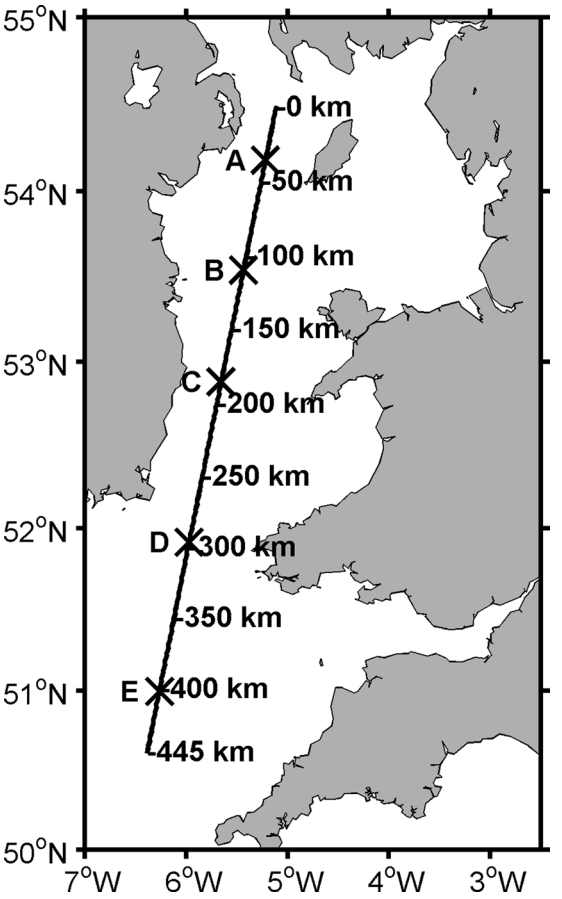

Figure 1. Map of the Irish Sea region (including St. George's Channel) showing the longitudinal transect and the positions (A–E) for which time series observations were collected.

A promising alternative to modeling studies is offered by optical remote sensing, since mineral particles suspended in the water column have a detectable effect on spectral reflectance even at relatively low concentrations [*Wozniak and Stramski*, 2004; *Gohin et al*., 2005]. Two classes of inversion algorithms exploit this effect. The first are single-band algorithms, which use red or near infra-red reflectance for the quantitative recovery of mineral particle concentrations [*Binding et al*., 2003; *Nechad et al*., 2010; *Neil et al*., 2011]. The second are variants of the "quasi-analytical algorithm" [*Lee et al*., 2002, 2005a, 2005b, 2013; *Mitchell et al*., 2014a], which provide validated procedures for obtaining the coefficients of absorption $a(\lambda)$ and backscattering $b_b(\lambda)$ from remote sensing reflectance in optically complex waters [*Shang et al*., 2011; *Zhao et al*., 2013; *Saulquin et al*., 2013; *Latha et al*., 2013; *Mitchell et al*., 2014b].

In this paper, we explore the possibility of combining these two types of algorithm to gain information on the relationship between sea surface reflectance, the optical properties and seasonal dynamics of suspended mineral particles, and light attenuation in the surface mixed layer. The potential advantages of this approach include a reduced requirement for the resource-intensive sampling of offshore waters and a degree of spatial and seasonal coverage that greatly exceeds that which can be achieved by ship-based surveys or autonomous vehicle deployments.

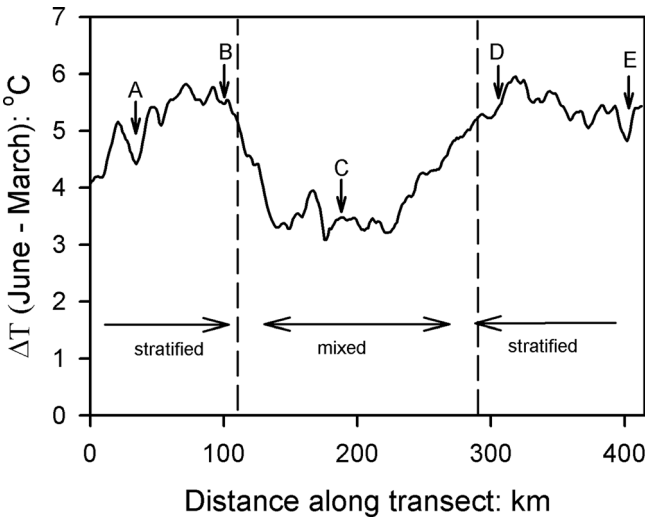

Figure 2. Change in MODIS sea surface temperature (ΔT) from March to June averaged over 8 years, with the approximate boundaries between cooler mixed and warmer seasonally stratified waters indicated.

2. Methodology

2.1. Location

Figure 1 shows a map of the Irish Sea and St George's Channel area, which is used here as a case study, with a transect drawn roughly from North to South. Single-pass MODIS remote sensing observations along this transect were processed to provide information on spatial variability in the deeper offshore waters of the region, while data from the individual locations labeled A, B, etc. were used to construct multiyear time series. A number of previous studies of the optical properties and optically significant constituents in this region have been published [*Bowers and Mitchelson-Jacobs*, 1996; *McKee and Cunningham*, 2006; *Tilstone et al*., 2005; *Neil et al*., 2011]. In the offshore waters occupied

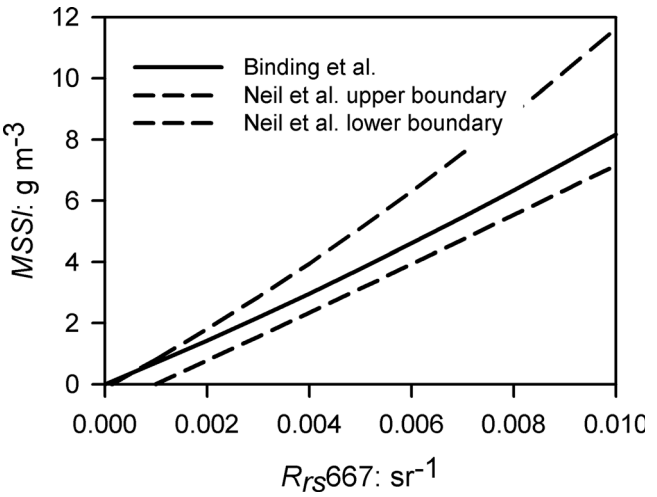

Figure 3. Relationships between suspended lithogenic mineral concentrations (*MSSI*) in the surface layer and remote sensing reflectance at 667 nm ($R_{rs}667$) derived from previous Irish Sea studies. The solid line shows results from the single-band algorithm derived by *Binding et al.* [2003] from in situ observations, and the broken lines indicate the upper and lower boundary values estimated by *Neil et al.* [2011] using radiative transfer modeling.

by the transect, concentrations of colored dissolved organic matter (CDOM, measured as the absorption coefficient at 440 nm of samples passed through a 0.2 μm filter) are consistently below 0.2 m^{-1}. Concentrations of mineral particles measured in spring and summer are generally in the range 1–4 g m^{-3} [*Bowers and Mitchelson-Jacobs*, 1996; *McKee and Cunningham*, 2006]. In winter, mineral particle concentrations have been reported to be significantly higher due to the resuspension of benthic sediments [*Bowers*, 2003], but this information is derived from Advanced Very High Resolution (AVHRR) satellite observations. Analysis of surface (1 m depth) samples taken at 110 stations in the Irish Sea at times extending from April to November, which cover most of the area of interest [see *Neil et al.*, 2011] (Figure 1), indicates that there is no discernible covariation between the concentrations of colored dissolved organic matter and suspended mineral particles ($R^2 = 0.02$) and that the organic fraction decreases as the total suspended material concentration increases in a manner which can be approximately described by a power law of the form $y = 0.6x^{-0.4}$. Mean values reported for chlorophyll *a* along the transect are around 2.2 mg m^{-3} in summer with occasional peaks of the order of 10 mg m^{-3} [*McKee and Cunningham*, 2006; *Gowen et al.*, 2008]. In winter, the waters of the Irish Sea and St. George's Channel are mixed by a combination of wind and tidal effects [*Bowers*, 2003], but in spring and summer thermally stratified regions form in the north (to the west of the Isle of Man) and in the south (as a continuation of the strongly stratified Celtic Sea). The positions of the tidal fronts which separate these different mixing regimes are marked by sharp gradients in sea surface temperature in early summer [*Pingree and Griffiths*, 1978; *Simpson and Bowers*, 1981; *Joint Nature Conservation Committee* (*JNCC*), 2004; *Souza*, 2013].

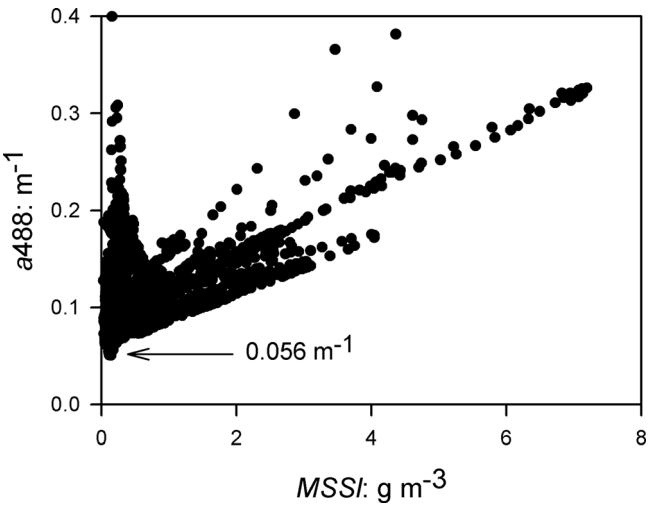

Figure 4. Absorption coefficients in the 488 nm waveband (*a*488) plotted against the concentration of lithogenic mineral particles (*MSSI*) determined by remote sensing for seven individual transects acquired over the period 7 April 2007 to 12 February 2008. The arrow indicates the value of the average *y* axis intercept attributable to nonparticulate absorption.

2.2. Remote Sensing Data

MODIS Aqua data for the 8 year period from January 2005 to December 2013 were downloaded from the NASA Goddard Distributed Active Archive Center. Level-1A data were processed in SeaDAS 6.4, using the default two-band aerosol model with iterative near infra-red correction, and mapped on a Mercator projection to obtain remote sensing reflectance $R_{rs}(\lambda)$ at 1 km resolution in the visible wavebands. Time series were created for the positions labeled A, B, C, etc. in Figure 1 by averaging observations within 11 × 11 pixel patches (corresponding to approximately 8.5 km × 12 km at the sea surface) whenever a minimum of 60 cloud-free pixels (~50% of the patch area) were available. The number of days when this criterion was met varied from 772 at station A to 894 at station D. Over

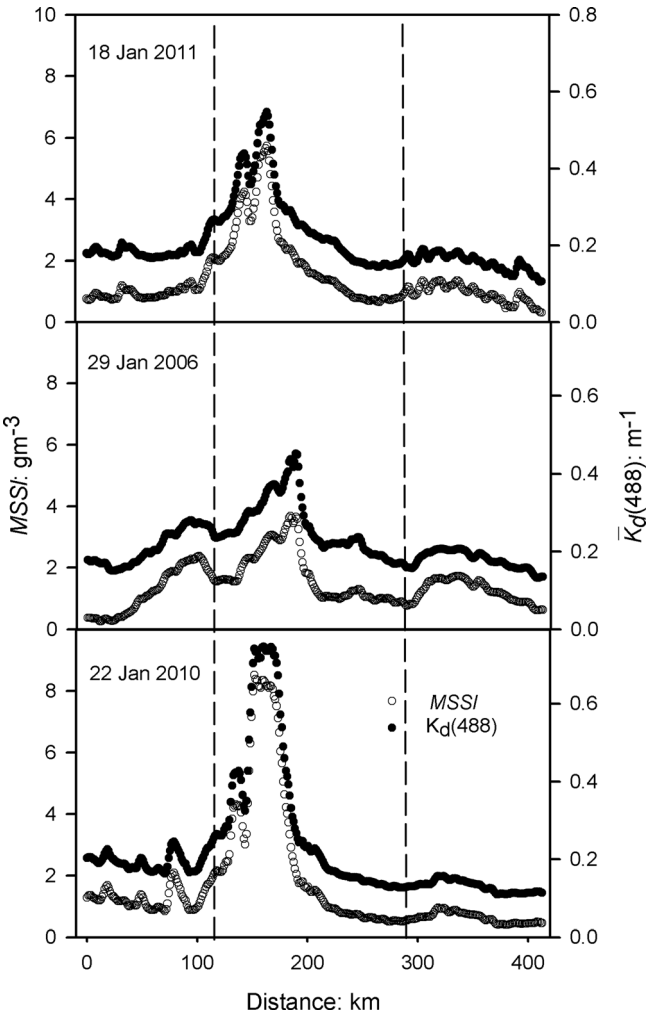

Figure 5. Mean attenuation coefficients for downward irradiance at 488 nm, $\bar{K}_d(488)$, and concentrations of lithogenic mineral particles (*MSSI*) extracted from three cloud-free MODIS images acquired in January (winter) in different years. The broken lines in this figure and the two which follow correspond to the boundaries between mixed and stratified regions drawn in Figure 2.

the same 8 year period, 47 days were identified where it was possible to generate transects of cloud-free reflectance observations from single satellite overpasses running along the line drawn in Figure 1. For these transects, data were averaged across a width of three pixels.

In addition, MODIS-derived sea surface temperatures were used to calculate the change in the average temperature of the surface layer along the transect line between the months of March and June, which provides a useful indication of the differences in vertical mixing depth which develop along the transect due to seasonal stratification. The approximate locations of the transitions between mixed and stratified regions derived in this way are shown in Figure 2 and repeated in the other figures which display transect data.

2.3. Mineral Particle Concentrations

A number of studies have shown that there is a monotonic (but nonlinear) relationship between the mass concentration of lithogenic minerals, *MSSI*, and red waveband remote sensing reflectance, $R_{rs}(\lambda)$ [*Binding et al*., 2003; *Nechad et al*., 2010; *Neil et al*., 2011], and two of these studies specifically considered the form taken by this relationship in the Irish Sea. *Neil et al*. [2011] carried out radiative transfer calculations which incorporated locally determined specific inherent optical properties to derive the upper (*u*) and lower (*l*) boundaries of the relationship between *MSSI* and $R_{rs}667$ in circumstances where the concentrations of colored dissolved organic matter (*CDOM*) and phytoplankton chlorophyll (*CHL*) were unknown (but within the ranges 0–1 m^{-1} for *CDOM* and 0–10 mg m^{-3} for *CHL*). From this modeling study, they proposed the relationships

$$MSSI_{(u)} = 26014 \times (R_{rs}667)^2 + 916 \times R_{rs}667 - 0.13, \quad (1)$$

$$MSSI_{(l)} = 2508 \times (R_{rs}667)^2 + 768 \times R_{rs}667 - 0.77. \quad (2)$$

Binding et al. [2003], on the other hand, carried out a ship-based study in which they measured subsurface irradiance reflectance at 665 nm in situ and sampled suspended mineral concentrations by determining the mass of particulate material retained on glass fiber filters after combustion. They derived a polynomial relationship which, when reformulated in terms of above-surface remote sensing reflectance ($R_{rs}665$: sr^{-1}) and lithogenic mineral concentrations (*MSSI*: g m^{-3}), takes the form

$$MSSI = 12549 \times (R_{rs}665)^2 + 649 \times R_{rs}665 + 1.74, \quad (3)$$

where the 665 nm waveband is sufficiently close to the MODIS 667 nm channel to allow a simple substitution. Binding et al. noted that the right-hand term in this relationship is problematic, since it gives a finite *MSSI* value at zero reflectance.

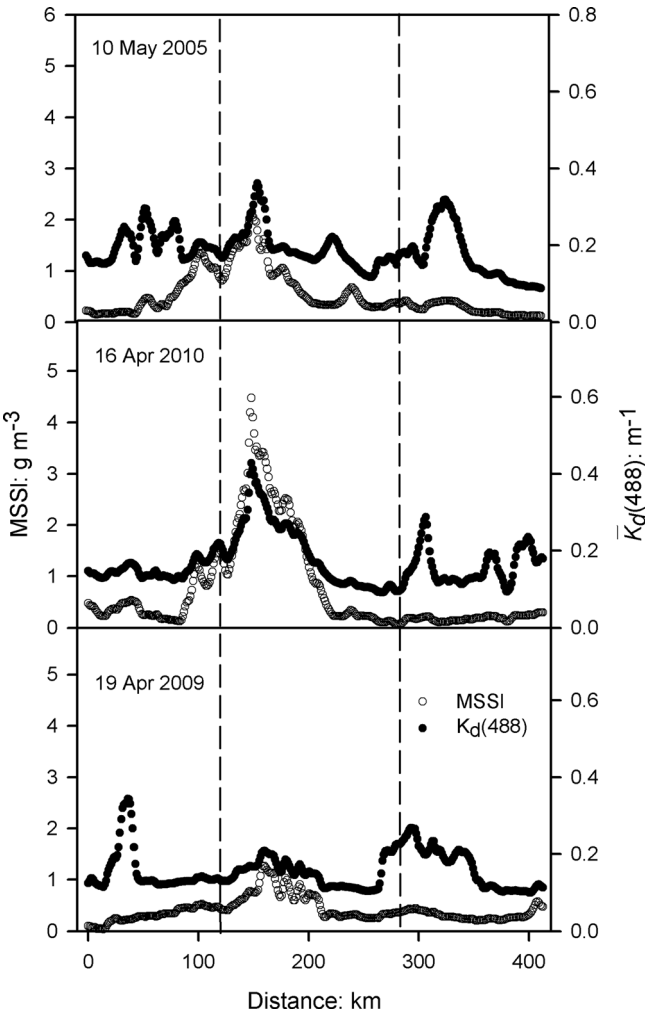

Figure 6. Mean attenuation coefficients for downward irradiance at 488 nm, $\bar{K}_d(488)$, and concentrations of lithogenic mineral particles (*MSSI*) from three cloud-free MODIS images acquired in late April/early May (spring) in different years.

Interestingly, *Nechad et al.* [2010] found an analogous offset in their analysis of North Sea data and argued that such offsets originate from systematic measurement errors and should be discounted. If, following Nechad et al. the final term is set to zero, equation (3) gives values which lie between the upper and lower limits proposed by Neil et al. (Figure 3). This makes sense, since measured *CDOM* and *CHL* values in the Irish Sea and adjacent waters (excepting eutrophicated coastal areas) fall well within the ranges used in the Neil et al. modeling study [*Gowen and Bloomfield*, 1996, *Gowen et al.*, 2008; *Bowers et al.*, 2013]. We have therefore used the expression

$$MSSI = 12549 \times (R_{rs}667)^2 + 649 \times R_{rs}667 \quad (4)$$

to generate remotely sensed MSS_I values for the present study.

2.4. Water Column Optics

The total absorption and backscattering coefficients of the surface layer were recovered from remote sensing reflectance spectra using version 5 of the Quasi Analytical Algorithm (QAAv5) proposed by *Lee et al.* [2009], with an additional step to linearize the recovered absorption coefficients and optimize performance for the Irish Sea. Details of the derivation and validation of this additional step may be found in *Mitchell et al.* [2014b]. Once the absorption and backscattering coefficients, $a(\lambda)$ and $b_b(\lambda)$, and the solar zenith angle in air, θ_a, are known, it is possible to calculate the average value of the attenuation coefficient for downward irradiance, $\bar{K}_d(\lambda)$, from the surface to the depth at which the irradiance reaches 10% of its surface value. A number of expressions have been proposed for this purpose [*Lee et al.*, 2005a, 2013], the simplest of which is

$$\bar{K}_d(\lambda) = (1 + 0.005\theta_a)a(\lambda) + 3.47 b_b(\lambda), \quad (5)$$

while and a more complex version with claimed improvements in accuracy takes the form

$$\bar{K}_d(\lambda) = (1 + m_0\theta_a)(a(\lambda) + m_1(1 - \gamma\eta_w(\lambda))(1 - m_2 e^{-m_3 a(\lambda)})b_b(\lambda), \quad (6)$$

where $m_0 = 0.005$, $m_1 = 4.259$, $m_2 = 0.52$, $m_3 = 10.8$, and $\gamma = 0.265$.

The performance of equations (5) and (6) was assessed using measurements made at 145 stations in the Irish Sea. Values for $a(\lambda)$ and $b_b(\lambda)$ were derived by applying the modified QAA to measurements of subsurface remote sensing reflectance made with a SeaWiFS Profiling Multichannel Radiometer (SPMR, Satlantic). These values were then used to calculate $\bar{K}_d(\lambda)$ by fitting straight lines to log-transformed measurements of downward planar irradiance and the results compared to those measured in situ using the same instrument. In the

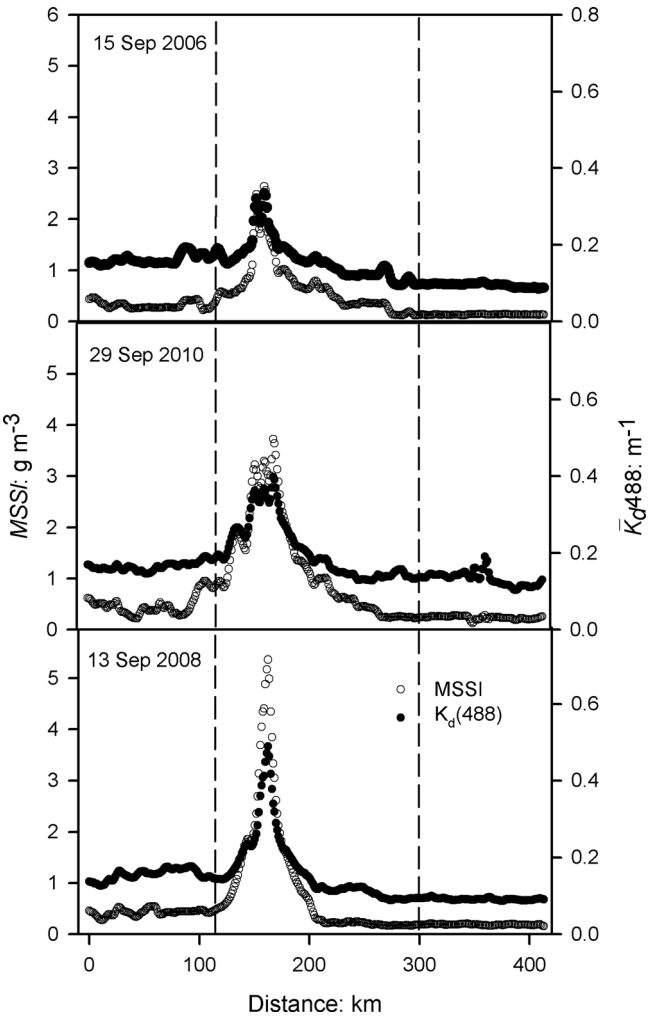

Figure 7. Mean attenuation coefficients for downward irradiance at 488 nm, $\bar{K}_d(488)$, and concentrations of lithogenic mineral particles (*MSSI*) from three cloud-free MODIS images acquired in September (autumn) in different years.

SPMR 490 nm waveband, which is the close to the MODIS 488 nm band used in most of the work reported here, equations (5) and (6) produced effectively equivalent results with absolute values within 5% of each other. Both equations recovered $\bar{K}_d(490)$ for a measured range from 0.06 to 1.32 m^{-1} with an RMS percentage error of 18%. Equation (5), however, offers the advantage that it can be easily rearranged to provide separate terms for the contributions of individual seawater constituents. If we write the total absorption and backscattering coefficients as the sum of the contributions of lithogenic minerals (*MSSI*) and other seawater constituents (*other*), so that

$$a(\lambda)=a_{MSSI}(\lambda)+a_{other}(\lambda), \quad (7)$$

and

$$b_b(\lambda)=b_{bMSSI}(\lambda)+b_{bother}(\lambda), \quad (8)$$

then equation (5) can be written

$$\bar{K}_d(\lambda)=[1.005\theta_a a_{MSSI}(\lambda)+3.47 b_{bMSSI}(\lambda)] +[1.005\theta_a a_{other}(\lambda)+3.47 b_{bother}(\lambda)]. \quad (9)$$

Furthermore, since the absorption and backscattering coefficients for mineral particles can be calculated as the product of particle concentration and the appropriate specific inherent optical properties, a^*_{MSSI} and $b_b{}^*_{MSSI}$, we have

$$\bar{K}_d(\lambda)=\left[1.005\theta_a a^*_{MSSI}(\lambda)MSSI+3.47 b^*_{bMSSI}(\lambda)MSSI\right] +[1.005\theta_a a_{other}(\lambda)+3.47 b_{bother}(\lambda)]=\bar{K}_{dMSSI}(\lambda)+\bar{K}_{dother}(\lambda), \quad (10)$$

which allows $\bar{K}_{dMSSI}(\lambda)$, the separate contribution of *MSSI* to $\bar{K}_d(\lambda)$, to be calculated if a^*_{MSSI} and $b_b{}^*_{MSS}$ are known.

2.5. Specific Inherent Optical Properties

In cases where mineral particles are the main determinant of remote sensing reflectance, the specific absorption and scattering cross sections $a^*_{MSSI}(\lambda)$ and $b^*_{bMSSI}(\lambda)$ can be estimated from the particulate components of the total absorption and backscattering coefficients $a_p(\lambda)$ and $b_{bp}(\lambda)$ using

$$a^*_{MSSI}(\lambda)=a_p(\lambda)/MSSI, \quad (11)$$

$$b^*_{bMSSI}(\lambda)=b_{bp}(\lambda)/MSSI. \quad (12)$$

The particulate backscattering coefficient, $b_{bp}(\lambda)$, can be derived from $b_b(\lambda)$ by simply subtracting the backscattering coefficient for the clearest oceanic waters [*Smith and Baker*, 1981]. However, in order to estimate the particulate absorption coefficient, it is necessary to subtract both the known water component [*Pope and Fry*, 1997] and an unknown CDOM contribution. The method adopted to determine the CDOM contribution in the 488 nm waveband was to plot $a(488)$ recovered using the QAA against *MSSI* (488) obtained using equation (4) for seven remote sensing

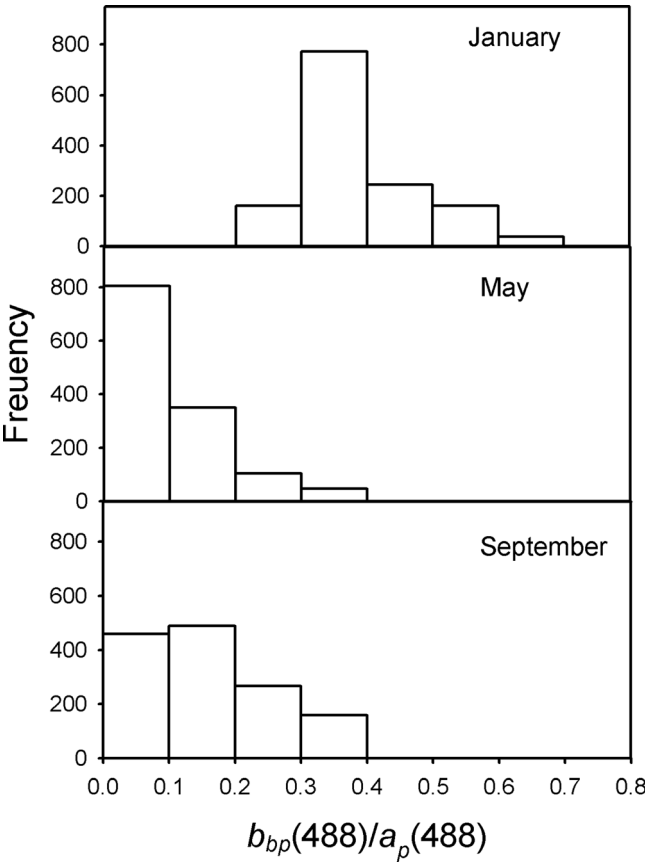

Figure 8. Seasonal changes in the distribution of particulate backscattering to absorption ratios in the 488 nm waveband. The histograms were derived from the transect data plotted in Figures 5–7.

transects acquired over the period 7 April to 8 February (Figure 4). The intercept of these plots on the *y* axis (i.e., the apparent absorption coefficient when no mineral particles were present) ranged from 0.04 to 0.06 m^{-1} with an average value of 0.056 m^{-1}. Part of this intercept could be accounted for by water absorption (approximately 0.015 m^{-1} at 488 nm) and the remaining 0.035 m^{-1} was attributed to CDOM (though there could be a small contribution from systematic errors). The CDOM contribution estimated in this way is around half of the value (after wavelength adjustment) of 0.07 m^{-1} suggested by *Bowers et al.* [2013], but closer to the in situ observations of 0.05 m^{-1} made by *Tilstone et al.* [2005]. Using a different remote sensing method, *Mitchell et al.* [2014b] estimated values of around 0.024 m^{-1} for this region.

3. Results

3.1. Transects

Examples of observations of *MSSI* and $\bar{K}_d(488)$ for the Irish Sea transect derived from MODIS overpasses on three separate days in winter are shown in (Figure 5), spring (Figure 6), and autumn (Figure 7). It was necessary to use days from different years for these plots due to cloud cover, but this has the advantage of showing the interannual consistency of the patterns that are observed. In winter and autumn, when tidal stirring is augmented by wind inputs [*Bowers*, 2003], *MSSI* values are elevated throughout the Irish Sea, peaking in the central region (Figure 5). The similarity in the shapes of the *MSSI* and $\bar{K}_d(488)$ plots at this time of year implies that mineral particles are the dominant determinant of irradiance attenuation. By late spring (Figure 6), values of both variables have fallen significantly throughout the length of the transect, indicating a loss of mineral particles from the surface layer. Moreover, the *MSSI* and $\bar{K}_d(488)$ curves are no longer correlated in the northern and southern sections, where ship surveys show that spring phytoplankton blooms are triggered by the onset of seasonal stratification [*Savidge*, 1976; *Gowen and Bloomfield*, 1996; *O'Boyle and Silke*, 2010]. In autumn, as stratification breaks down, *MSSI* in the central region increases and the correlation with $\bar{K}_d(488)$ is restored (Figure 7). Since the ratio of the backscattering coefficient to the absorption coefficient is typically higher for mineral particles than for phytoplankton cells [*Sullivan et al.*, 2005; *McKee and Cunningham*, 2006], these ratios can provide information on seasonal variations in the composition of the suspended particle population. Histograms of $b_{bp}488/a_p488$ calculated from the transect observations (with the assumption of a constant CDOM contribution to the total water column absorption coefficient of 0.035 m^{-1}) are therefore plotted in Figure 8. The January data show the presence of particles with a relatively high ratio of backscattering to absorption, and support the argument that resuspended benthic minerals are the main constituent of the Irish Sea particle assemblage in winter [*Bowers*, 2003]. A reduction in $b_{bp}488/a_p488$ in summer coincides with the loss of mineral particles from the surface layer and an increased contribution by phytoplankton cells, while the histogram for September shows the particle population in a state of transition toward the higher $b_{bp}488/a_p488$ values characteristic of winter conditions. The optical dominance of mineral particles in winter is strikingly

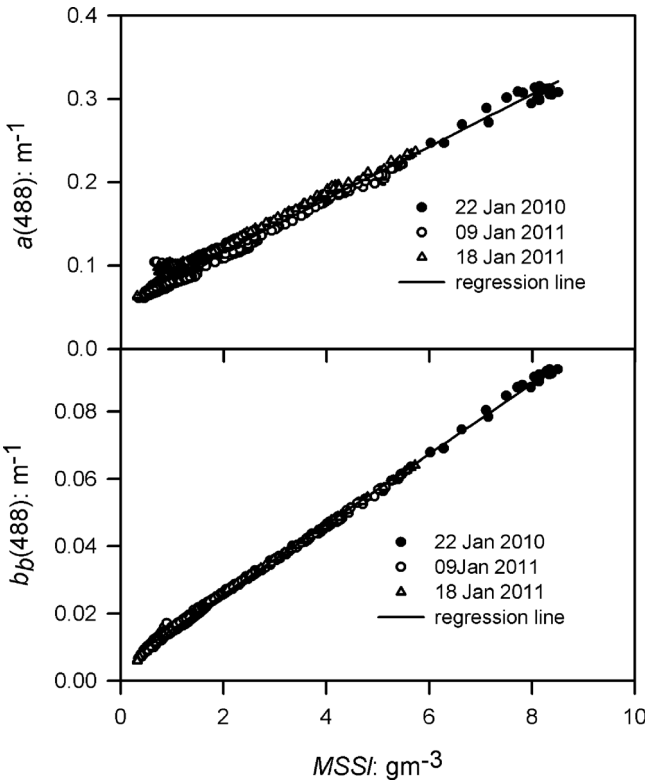

Figure 9. Relationships between satellite-derived absorption and backscattering coefficients at 488 nm, $a(488)$, and $b_b(488)$, and concentrations of mineral suspended solids (*MSSI*) for transects acquired during three clear January days. The gradients of the lines fitted to the data by least squares regression provide an estimate of the specific absorption and backscattering coefficients for mineral particles, a^*_{MSS} 488 and $b_b{}^*_{MSS}$ 488.

illustrated by the strong correlation between $a488$ and *MSSI* and b_b488 and *MSSI* in data from the three January transects plotted in Figure 9. The regression lines fitted through these data have equations

$$a488 = 0.031 MSSI + 0.054, \quad (13)$$

and

$$b_b488 = 0.010 MSSI + 0.005, \quad (14)$$

with correlation coefficients close to unity, and their gradients provide values of $a^*_{MSSI}488 = 0.031$ m^2 g^{-1} for the specific absorption cross section and $b_b{}^*_{MSSI}488 = 0.010$ m^2 g^{-1} for the specific backscattering cross section of suspended lithogenic mineral particles in surface waters. The high correlation coefficients, and the consistency of observations obtained on different days, indicate that this method of determining SIOPs is surprisingly free of random errors. While the possible existence of significant systematic errors cannot be ruled out, they cannot be estimated from the plots in Figure 9. The results obtained by remote sensing are, however, encouragingly close to the values of a^*_{MSSI} 488 = 0.04 m^2 g^{-1} and $b_b{}^*_{MSSI} = 0.016$ m^2 g^{-1} derived by *Neil et al.* [2011] from ship-based sampling in the region.

3.2. Time Series

Eight years of MODIS observations were collated for the positions labeled A–E in Figure 1, and the resulting time series are plotted for *MSSI* in Figure 10 and $\bar{K}_d(488)$ in Figure 11. The *MSSI* data at all positions show clear seasonal cycles, with winter peaks and summer troughs. The height of the peaks is greatest at position C, where tidal currents are strongest. The duration of the low-MSS period in summer is significantly shorter at position C than at positions which seasonally stratify (A and E), which implies a shorter period in which the degree of vertical mixing falls below that required to maintain mineral particles in the surface layer. Since net phytoplankton growth in water columns which extend below the compensation depth depends on restricted vertical mixing, this may explain the observation that blooms in the offshore regions of the Irish Sea occur in summer, in contrast to the marked spring and autumn blooms in stratified waters [*Gowen and Bloomfield*, 1996].

Seasonal cycles are also evident in $\bar{K}_d(488)$ (Figure 11), and the regular pattern of vertical attenuation in the center of the transect (position C) clearly follows variations in suspended mineral concentrations. To the north and south, however (especially positions A and E) sharp upward excursions are observed in $\bar{K}_d(488)$ in spring and summer when *MSSI* values are low. Examination of changes in the backscattering to absorption ratio during these events [*Mitchell et al.*, 2014b] suggests that they are due to phytoplankton blooms. As a means of concisely summarizing spatial and temporal variations in the dependence of $\bar{K}_d(488)$ on *MSSI* along the transect, Pearson correlation coefficients (R) were calculated for the time series data (Figure 12). The influence of mineral particles on $\bar{K}_d(488)$ is greatest at position C ($R = 0.89$), where mixing persists throughout the year, and least at positions A ($R = 0.36$) and E ($R = 0.39$) where seasonal stratification occurs.

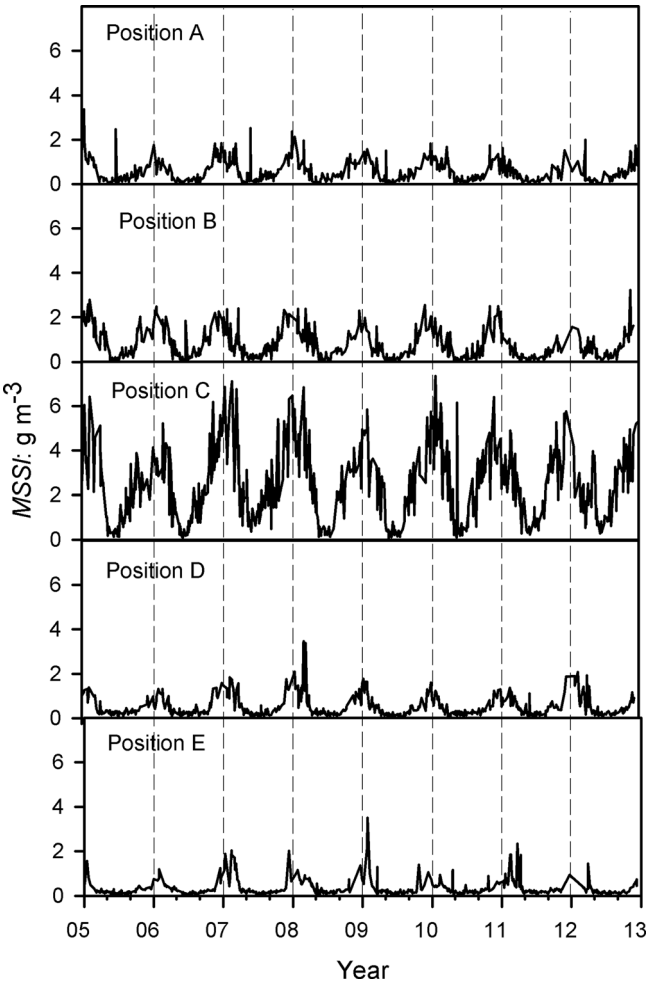

Figure 10. Eight year time series of *MSSI* concentrations recovered from MODIS observations using equation (4) for positions A–E, whose locations are indicated in Figure 1.

3.3. Mapping MSSI Contributions

Values for the depth-averaged attenuation coefficient for downward irradiance, $\bar{K}_d(488)$, were derived from remotely sensed $a488$ and b_b488 data using equation (5). The contributions of suspended mineral particles, $\bar{K}_{dMSSI}(488)$, were calculated using equation (10) using *MSSI* derived from red waveband reflectance (equation (4)) and SIOPs from the winter regression lines (equations (13) and (14)). As a test of consistency, $\bar{K}_{dMSSI}(488)$ was also calculated using the absorption partitioning method of *Mitchell et al.* [2014b], which was developed using year-round data with a bias toward spring and summer observations. The results from the two methods were very similar, with a root mean square difference of 0.01 m^{-1} and a correlation coefficient close to unity. Composite maps of the fractional mineral particle contribution, $\bar{K}_{dMSSI}(488)/\bar{K}_d(488)$ were drawn up in which each pixel contains the average of all available observations over an 8 year period for the months of January, April, July, and October (Figure 13). These maps provide important seasonal and spatial contexts for the transect and time series observations. As expected, the contribution of mineral particles to light attenuation in the water column is highest in winter (over 70%) and lowest in summer (below 20% for much of the region). In addition, however, a number of interesting details emerge. First, in the January map the contribution of *MSSI* to $\bar{K}_d(488)$ is closely related to bathymetry, being highest in coastal areas where the water column is shallow and lower over the deep trough which runs down the center of the Irish Sea [*JNCC*, 2004; *Souza*, 2013]. Second, the July image indicates that elevated *MSSI* contributions persist in summer in estuaries and in the areas off Anglesey (in NW Wales) and Wicklow Head (in SE Ireland) which were identified by *Bowers et al.* [2002] as sites of high (>1 m s^{-1}) tidal currents. Third, the patterns observed in spring and autumn (April and October) bear a striking resemblance to maps showing the location of mixed and seasonally stratified regions [*JNCC*, 2004; *Souza*, 2013], suggesting that the optical signals generated by mineral particles can clearly delineate the position of tidal fronts and provide a sensitive indicator of the degree of vertical mixing of the water column in the Irish Sea.

4. Discussion

In an attempt to present the underlying argument as clearly as possible, the results obtained by remote sensing have been presented above without a discussion of the uncertainties associated with the derived variables. Uncertainties in *MSSI* values estimated from $R_{rs}(665)$ using equation (4) arise from (i) variability in the relationship between $R_{rs}(665)$ and *MSSI* and (ii) errors in the recovery of $R_{rs}(665)$ from MODIS top-of-atmosphere observations. The degree of uncertainty in *MSSI* values due the presence of interfering substances (CDOM and phytoplankton cells), when $R_{rs}(665)$ values are measured in situ, is indicated by the upper

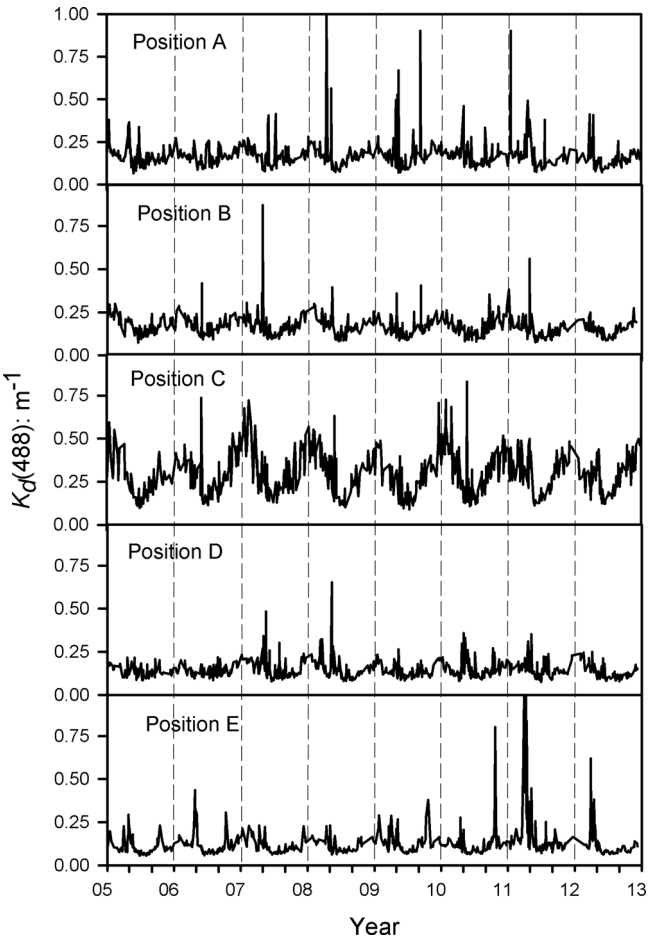

Figure 11. Eight year time series for $\bar{K}_d(488)$ calculated from MODIS observations using equation (5) for positions A–E whose locations are indicated in Figure 1.

and lower boundaries in Figure 3. These boundaries were derived by numerical modeling but are consistent with ship-based observations [*Binding et al.*, 2003; *Neil et al.*, 2011], and indicate uncertainties of around ±25% for *MSSI* concentrations of 5 g m^{-3}. Recent estimates suggest that standard MODIS atmospheric correction procedures can introduce errors of around ±30% in $R_{rs}667$ values in low-turbidity coastal waters [*Goyens et al.*, 2013; *Moore et al.*, 2015]. Assuming errors (i) and (ii) are independent, and combining them in quadrature, gives an overall figure of ±40% for *MSSI* retrievals based on equation (4). The procedure used to derive $K_d(490)$ involves the derivation of $a(488)$ and $b_b(488)$ as an intermediate step. Exploratory calculations indicate that the wavelength-dependent percentage errors derived by *Moore et al.* [2015] for MODIS R_{rs} values for shelf sea conditions typically contribute errors of 20% to $a(488)$ and $b_b(488)$ derived using QAAv5. This is sufficient to account for much of the spread in the ratios of particulate backscattering to absorption in this waveband noted in Figure 8, and taken in isolation would result in a 25% error in $K_d(488)$. If the 18% uncertainty obtained when the $K_d(488)$ procedure was validated using SPMR casts for the Irish Sea region is also taken into account, we have an estimated root mean square error of the order of 30% in $K_d(488)$ derived from atmospherically corrected MODIS observations. The absence of high spatial frequency noise of this magnitude in the transect data plotted in Figures 5–7, however, indicates that these estimated errors associated with *MSSI* and $K_d(488)$ recoveries do not operate on a pixel-by-pixel basis. They should probably be interpreted as indications of likely inaccuracies in absolute values rather than as disruptive influences on patterns derived from individual overpasses, but further work in separating out the effects of systematic and random errors in MODIS shelf-sea products is clearly required.

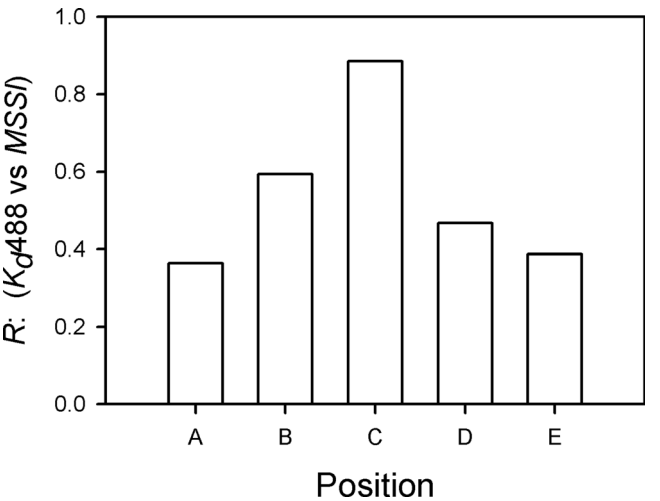

Figure 12. Variations in the Pearson correlation coefficient R between $\bar{K}_d(488)$ and *MSSI* for positions A–E, calculated for the time series data plotted in Figures 10 and 11.

In spite of these caveats, the availability of a long series of satellite observations means that it is now feasible to

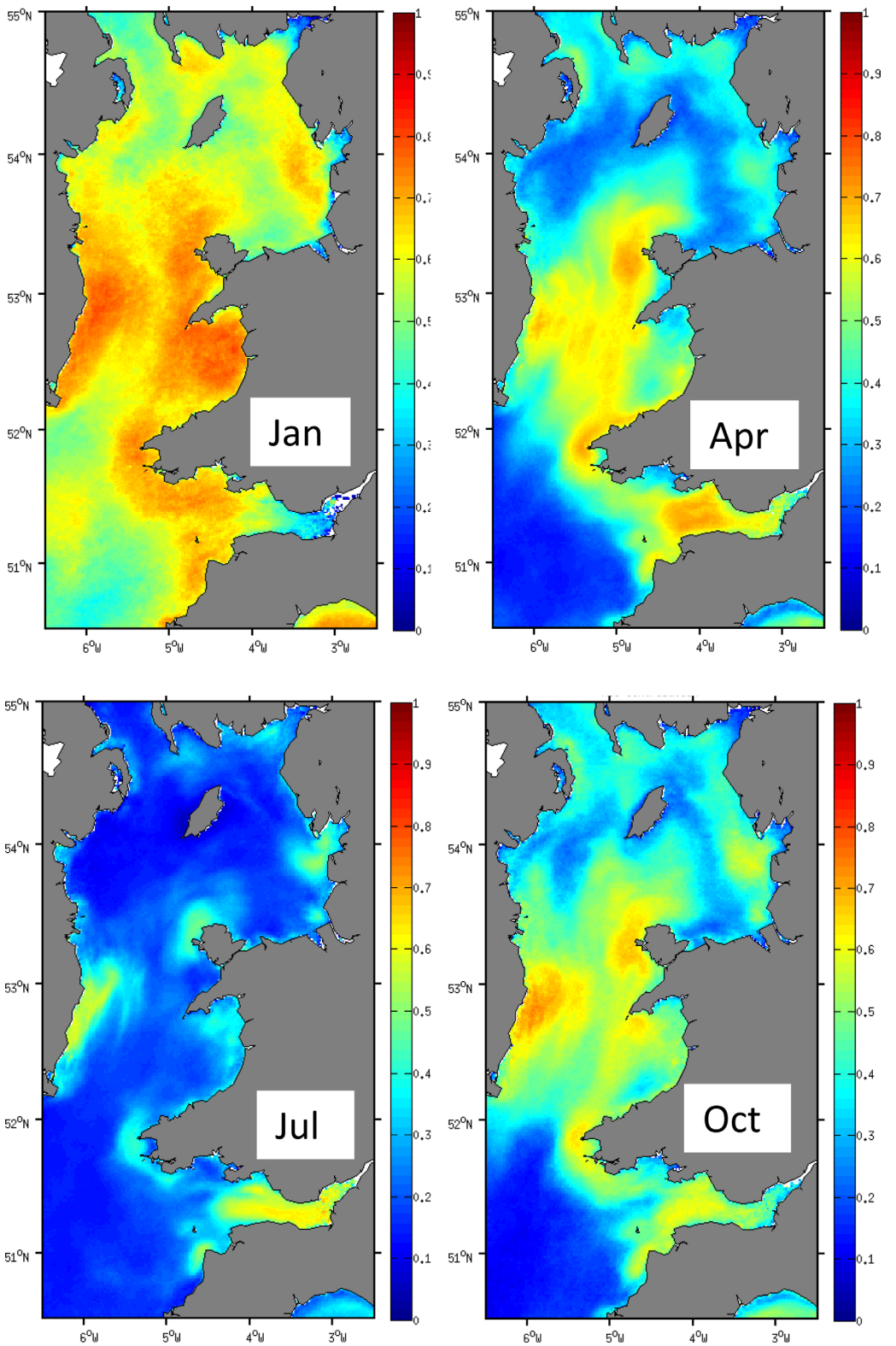

Figure 13. Composite maps showing the fractional contribution of *MSSI* to $\bar{K}_d(488)$, calculated for the calendar months of January, April, July, and October all available observations over the 8 year time period.

use remote sensing to study the seasonal and spatial variability of suspended particle populations even in cloudy regions such as the Irish Sea. These studies are important because the relatively low mineral particle concentrations found in offshore waters can have significant optical effects which include an increase in the rate of light attenuation in the water column [*Devlin et al*., 2008], the degradation of underwater visibility [*Hou et al*., 2008], impairment of the performance of chlorophyll retrieval algorithms [*Tzortziou et al*., 2007] and a reduction in the penetration depth for passive and active remote sensing techniques [*Gordon and McCluney*, 1975]. Foreseeable applications of the techniques evaluated in this paper include studies of particle-mediated pollutant transport [*Charlesworth et al*., 2006; *Huang et al*., 2013], vertical mixing patterns induced by storms and other episodic events [*Sosik et al*., 2001] and the provision of a link between suspended mineral concentrations and light attenuation coefficients in shelf sea ecosystem models [*Wan et al*., 2013]. In the case of the Irish Sea, the lowest summer value for $\bar{K}_d(488)$ is approximately 0.1 m^{-1} and the highest winter value around 0.7 m^{-1}. This difference, which is largely due to changes in the concentration of mineral particles in surface waters, corresponds to a reduction in the penetration depth for the 488 nm waveband from 10 to 1.4 m, and in the euphotic depth from 40 to 7.5 m [*Mitchell and Cunningham*, 2015]. A key finding in the present study is the possibility of using winter observations to derive specific absorption and backscattering coefficients for lithogenic minerals at a time when the particle population consists almost exclusively of this material [*Bowers*, 2003] and energetic turbulence is likely to produce the maximum degree of particle disaggregation [*Braithwaite et al*., 2012; *Markussen and Andersen*, 2014]. This remote sensing method of determining SIOPs is not error-free, but it avoids artifacts associated with sample preparation and handling and the uncertain choice of beta factor correction for absorption measurements carried out using filter papers. The SIOPs obtained are of considerable value for modeling studies: in situ determinations of specific backscattering coefficients in particular often have wide margins of error [*Snyder et al*., 2008]. Of course, caution is required in extrapolating the values of the SIOPs obtained for the Irish Sea to other regions, but the method employed here is applicable to low-turbidity shelf seas wherever they occur. For the Irish Sea and adjacent waters, the general pattern of increased levels of *MSSI* in winter and reduced levels in summer is neatly explained by the resuspension model proposed by *Bowers* [2003], which takes into account turbulent energy inputs due to both tides and winds. Variations in the details of this pattern along the transect can be related to different vertical mixing regimes. For example, there is a rapid loss of mineral particles from surface waters in stratifying regions in spring while in mixed regions minimum *MSSI* values are reached around midsummer. Finally, the divergence of remotely sensed *MSSI* and $\bar{K}_d(488)$ curves at the northern and southern ends of the transect in spring and summer (Figure 6) indicates that the suggestion by *Devlin et al*. [2008] that light attenuation in UK shelf seas can be directly estimated from suspended sediment concentrations should be treated with caution in offshore waters.

Acknowledgments
This work was partly funded by a UK Natural Environment Research Council Studentship held by Catherine Mitchell. Processed satellite data are available on request from the Marine Optics and Remote Sensing Laboratory at the University of Strathclyde, Glasgow, Scotland.

References

Agrawal, Y. C., and H. C. Pottsmith (2000), Instruments for particle size and settling velocity observations in sediment transport, *Mar. Geol.*, *168*, 89–114.

Astoreca, R., D. Doxaran, K. Ruddick, V. Rousseau, and C. Lancelot (2012), Influence of suspended particle concentration, composition and size on the variability of inherent optical properties of the Southern North Sea, *Cont. Shelf Res.*, *35*, 117–128.

Babin, M., A. Morel, V. Fournier-Sicre, F. Fell, and D. Stramski (2003), Light scattering properties of marine particles in coastal and open ocean waters as related to the particle mass concentration, *Limnol. Oceanogr.*, *48*, 843–859.

Binding, C. E., D. G. Bowers, and E. G. Mitchelson-Jacob (2003), An algorithm for the retrieval of suspended sediment concentrations in the Irish Sea from SeaWiFS ocean colour satellite imagery, *Int. J. Remote Sens.*, *24*, 3791–3806.

Bowers, D. G. (2003), A simple turbulent energy-based model of fine suspended sediments in the Irish Sea, *Cont. Shelf Res.*, *23*, 1495–1505.

Bowers, D. G., and E. G. Mitchelson-Jacobs (1996), Inherent optical properties of the Irish Sea determined from underwater irradiance measurements, *Estuarine Coastal Shelf Sci.*, *43*, 433–447.

Bowers, D. G., S. Gaffney, M. White, and P. Bowyer (2002), Turbidity in the Southern Irish Sea, *Cont. Shelf Res.*, *22*, 2115–2126.

Bowers, D. G., E. M. Roberts, M. White, and B. D. Moate (2013), Water masses, mixing, and the flow of dissolved organic carbon through the Irish Sea, *Cont. Shelf Res.*, *8*, 12–20.

Braithwaite, K. M., D. G. Bowers, W. A. M. N. Smith, and G. W. Graham (2012), Controls on floc growth in an energetic tidal channel, *J. Geophys. Res.*, *117*, C02024, doi:10.1029/2011JC007094.

Charlesworth, M. E., S. Chenery, A. Mellor, and M. Service (2006), Isotopic composition and concentration of Pb in suspended particulate matter of the Irish Sea reveals distribution and sources, *Mar. Pollut. Bull.*, *52*, 81–88.

Devlin, M. J., J. Barry, D. K. Mills, R. J. Gowen, J. Foden, D. Sivyer, and P. Tett (2008), Relationships between suspended particulate material, light attenuation and Secchi depth in UK marine waters, *Estuarine Coastal Shelf Sci.*, *79*, 429–439.

Downing, J. (2006), Twenty-five years with OBS sensors: The good, the bad, and the ugly, *Cont. Shelf Res.*, *26*, 2299–2318.

Fettweis, M. P., and B. Nechad (2011), Evaluation of in situ and remote sensing sampling methods for SPM concentrations, Belgian continental shelf (southern North Sea), *Ocean Dyn.*, *61*, 157–171.

Gohin, F., S. Loyer, M. Lunven, C. Labry, J. Froidefond, D. Delmas, M. Huret, and A. Herbland (2005), Satellite-derived parameters for biological modelling in coastal waters: Illustration over the eastern continental shelf of the Bay of Biscay, *Remote Sens. Environ.*, *95*, 29–46.

Gordon, H. R., and W. R. McCluney (1975), Estimation of the depth of sunlight penetration in the sea from remote sensing, *Appl. Opt.*, *14*, 413–416.
Gowen, R. J., and S. P. Bloomfield (1996), Chlorophyll standing crop and phytoplankton production in the western Irish Sea during 1992 and 1993, *J. Plankton Res.*, *18*, 1735–1751.
Gowen, R. J., P. Tett, K. Kennington, D. K. Mills, T. M. Shammon, B. M. Stewart, N. Greenwood, C. Flanagan, M. Devlin, and A. Wither (2008), The Irish Sea: Is it eutrophic?, *Estuarine Coastal Shelf Sci.*, *76*, 239–254.
Goyens, C., C. Jamet, and T. Schroeder (2013), Evaluation of four atmospheric correction algorithms for MODIS-Aqua images over contrasted coastal waters, *Remote Sens. Environ.*, *131*, 63–75.
Hou, W. L., D. J. Gray, A. D. Weidemann, and R. A. Arnone (2008), Comparison and validation of point spread models for imaging in natural waters, *Opt. Express*, *16*, 9958–9965.
Huang, D. K., J. Z. Du, B. Deng, and J. Zhang (2013), Distribution patterns of particle-reactive radionuclides in sediments off eastern Hainan Island, China: Implications for source and transport pathways, *Cont. Shelf Res.*, *57*, 10–17.
Joint Nature Conservation Committee (JNCC) (2004), The Irish Sea Pilot, final report, 172 pp., Peterborough, U. K.
Kostadinov, T. S., D. A. Siegel, S. Maritorena, and N. Guillocheau (2012), Optical assessment of particle size and composition in the Santa Barbara Channel, California, *Appl. Opt.*, *51*, 3171–3189.
Latha, T. P., P. V. Nagamani, B. S. Rao, P. Amarendra, K. H. Rao, S. B. Choudhury, S. K. Dash, and V. V. S. S. Sarma (2013), Particle backscattering variability in the coastal waters of Bay of Bengal: A case study along off Kakinada and Yanam regions, *IEEE Geosci. Remote Sens. Lett.*, *10*, 1517–1521.
Lee, Z., C. Hu, S. Shang, K. Du, M. Lewis, R. Arnone, and R. Brewin (2013), Penetration of UV-visible solar radiation in the global oceans: Insights from ocean color remote sensing, *J. Geophys. Res. Oceans*, *118*, 4241–4255, doi:10.1002/jgrc.20308.
Lee, Z. P., K. L. Carder, and R. A. Arnone (2002), Deriving inherent optical properties from water color: A multiband quasi-analytical algorithm for optically deep waters, *Appl. Opt.*, *41*, 5755–5772.
Lee, Z. P., K. P. Du, and R. Arnone (2005a), A model for the diffuse attenuation coefficient of downwelling irradiance, *J. Geophys. Res.*, *110*, C02016, doi:10.1029/2004JC002275.
Lee, Z. P., M. Darecki, K. L. Carder, C. O. Davis, D. Stramski, and W. J. Rhea (2005b), Diffuse attenuation coefficient of downwelling irradiance: An evaluation of remote sensing methods, *J. Geophys. Res.*, *110*, C02017, doi:10.1029/2004JC002573.
Lee, Z. P., B. Lubac, J. Werdell, and R. Arnone (2009), *An Update of the Quasi-Analytical Algorithm (QAAv5)*, Int. Ocean Colour Coord. Group, Dartmouth, Canada.
Lunau, M., A. Sommer, A. Lemke, H. P. Grossart, and M. Simon (2004), A new sampling device for microaggregates in turbid aquatic systems, *Limnol. Oceanogr. Methods*, *2*, 387–397.
Markussen, T. N., and T. J. Andersen (2014), Flocculation and floc break-up related to tidally induced turbulent shear in a low-turbidity, microtidal estuary, *J. Sea Res.*, *89*, 1–11.
McKee, D., and A. Cunningham (2006), Identification and characterisation of two optical water types in the Irish Sea from in situ inherent optical properties and seawater constituents, *Estuarine Coastal Shelf Sci.*, *68*, 305–316.
Mitchell, C., and A. Cunningham (2015), Remote sensing of spatio-temporal relationships between the partitioned absorption coefficients of phytoplankton cells and mineral particles and euphotic zone depths in a partially mixed shelf sea, *Remote Sens. Environ.*, *160*, 193–205.
Mitchell, C., A. Cunningham, and D. McKee (2014a), Remote sensing of shelf sea optical properties: Evaluation of a quasi-analytical approach for the Irish Sea, *Remote Sens. Environ.*, *143*, 142–153.
Mitchell, C., A. Cunningham, and D. McKee (2014b), Remote sensing of particulate absorption coefficients and their biogeochemical interpretation: A case study in the Irish Sea, *Remote Sens. Environ.*, *152*, 74–82.
Mobley, C. D. (1994), *Light and Water: Radiative Transfer in Natural Waters*, 592 pp., Academic, San Diego, Calif.
Moore, T. S., J. W. Campbell, and H. Feng (2015), Characterizing the uncertainties in spectral remote sensing reflectance for SeaWiFS and MODIS-Aqua based on global in situ matchup data sets, *Remote Sens. Environ.*, *159*, 14–27.
Nechad, B., K. G. Ruddick, and Y. Park (2010), Calibration and validation of a generic multisensor algorithm for mapping of total suspended matter in turbid waters, *Remote Sens. Environ.*, *114*, 854–866.
Neil, C., A. Cunningham, and D. McKee (2011), Relationships between suspended mineral concentrations and red-waveband reflectances in moderately turbid shelf seas, *Remote Sens. Environ.*, *115*, 3719–3730.
O'Boyle, S., and J. Silke (2010), A review of phytoplankton ecology in estuarine and coastal waters around Ireland, *J. Plankton Res.*, *32*, 99–118.
Pingree, R. D., and D. K. Griffiths (1978), Tidal fronts on the shelf seas around the British Isles, *J. Geophys. Res.*, *83*, 4615–4622.
Pope, R. M., and E. S. Fry (1997), Absorption spectrum (380–700 nm) of pure water. II. Integrating cavity measurements, *Appl. Opt.*, *36*, 8710–8723.
Saulquin, B., A. Hamdi, F. Gohin, J. Populus, A. Mangin, and O. F. d'Andon (2013), Estimation of the diffuse attenuation coefficient K_{dPAR} using MERIS and application to seabed habitat mapping, *Remote Sens. Environ.*, *128*, 224–233.
Savidge, G. (1976), Preliminary study of distribution of chlorophyll-a in vicinity of fronts in Celtic and western Irish Seas, *Estuarine Coastal Mar. Sci.*, *4*, 617–625.
Shang, S., Z. Lee, and G. Wei (2011), Characterization of MODIS-derived euphotic zone depth: Results for the China Sea, *Remote Sens. Environ.*, *115*, 180–186.
Simpson, J. H., and D. G. Bowers (1981), Models of stratification and frontal movement in shelf seas, *Deep Sea Res., Part A*, *28*, 727–738.
Smith, R. C., and K. S. Baker (1981), Optical properties of the clearest natural waters (200–800 nm), *Appl. Opt.*, *20*, 177–184.
Snyder, W. A., et al. (2008), Optical scattering and backscattering by organic and inorganic particulates in US coastal waters, *Appl. Opt.*, *47*, 666–677.
Sosik, H. M., R. E. Green, W. S. Pegau, and C. S. Roesler (2001), Temporal and vertical variability in optical properties of New England shelf waters during late summer and spring, *J. Geophys. Res.*, *106*, 9455–9472.
Souza, A. J. (2013), On the use of the Stokes number to explain frictional tidal dynamics and water column structure in shelf seas, *Ocean Sci.*, *9*, 391–398.
Stavn, R. H., and S. J. Richter (2008), Biogeo-optics: Particle optical properties and the partitioning of the spectral scattering coefficient of ocean waters, *Appl. Opt.*, *47*, 2660–2679.
Sullivan, J. M., M. S. Twardowski, P. I. Donaghay, and S. A. Freeman (2005), Use of optical scattering to discriminate particle types in coastal waters, *Appl. Opt.*, *44*, 1667–1680.
Tilstone, G. H., T. J. Smyth, R. J. Gowen, V. Martinez-Vicente, and S. B. Groom (2005), Inherent optical properties of the Irish Sea and their effect on satellite primary production algorithms, *J. Plankton Res.*, *27*, 1127–1148.

Tzortziou, M., A. Subramaniam, J. R. Herman, C. L. Gallegos, P. J. Neale, and L. W. Harding (2007), Remote sensing reflectance and inherent optical properties in the mid Chesapeake Bay, *Estuarine Coastal Shelf Sci.*, *72*, 16–32.

Van Oostende, N., J. Harlay, B. Vanelslander, L. Chou, W. Vyverman, and K. Sabbe (2012), Phytoplankton community dynamics during late spring coccolithophore blooms at the continental margin of the Celtic Sea (North East Atlantic, 2006–2008), *Prog. Oceanogr.*, *104*, 1–16.

Wan, Z. W., H. S. Bi, and J. She (2013), Comparison of two light attenuation parameterization focusing on timing of spring bloom and primary production in the Baltic Sea, *Ecol. Modell.*, *259*, 40–49.

Wozniak, S. B., and D. Stramski (2004), Modeling the optical properties of mineral particles suspended in seawater and their influence on ocean reflectance and chlorophyll estimation from remote sensing algorithms, *Appl. Opt.*, *43*, 3489–3503.

Zhang, X., R. H. Stavn, A. U. Falster, D. Gray, and R. W. Gould (2014), New insight into particulate mineral and organic matter in coastal ocean waters through optical inversion, *Estuarine Coastal Shelf Sci.*, *149*, 1–12.

Zhao, J., B. Barnes, N. Melo, D. English, B. Lapointe, F. Muller-Karger, B. Schaeffer, and C. M. Hu (2013), Assessment of satellite-derived diffuse attenuation coefficients and euphotic depths in south Florida coastal waters, *Remote Sens. Environ.*, *131*, 38–50.